Research Square

Preprints are preliminary reports that have not undergone peer review.
They should not be considered conclusive, used to inform clinical practice,
or referenced by the media as validated information.

Antifungal Activity of Zinc Oxide Nanoparticles against Cryptococcus neoformans: Cytotoxicity and Changes in CAP59 Transcript Abundance

Mona M. H. Soliman
National Research Centre
Mai M. Kandil
National Research Centre
Mohamed Seif
seif.eg@gmail.com

National Research Centre

Research Article

Keywords: Antifungal activity, Cryptococcus neoformans, CAP59, Cytotoxicity, One Health, Zinc oxide nanoparticles

Posted Date: November 23rd, 2026

DOI: https://doi.org/10.21203/rs.3.rs-11651730/v1

License: This work is licensed under a Creative Commons Attribution 4.0 International License.
Read Full License

Additional Declarations: No competing interests reported.

Antifungal Activity of Zinc Oxide Nanoparticles against *Cryptococcus neoformans*: Cytotoxicity and Changes in *CAP59* Transcript Abundance

Mona M. H. Soliman [1], Mai M. Kandil [1] and Mohamed Seif* [2]

[1] Microbiology and Immunology Department, National Research Centre, Giza, 12622, Egypt
[2] Food Toxicology and Contaminants Department, Food Industries and Nutrition Research Institute, National Research Centre, Giza, 12622, Egypt

***Corresponding Authors**

Mohamed Seif, (PhD.)

Associate Professor

Food Toxicology and Contaminants Department,
Food Industries and Nutrition Research Institute,
National Research Centre, Giza, 12622, Egypt.
Email: seif.eg@gmail.com
Tel: +2 01281052247

Abstract

Cryptococcus neoformans (*C. neoformans*) is an opportunistic environmental yeast associated with avian habitats, particularly pigeon droppings, representing a potential source of environmental exposure relevant to the One Health framework. This study investigated the occurrence and molecular characterization of C. neoformans in pigeon droppings collected in Cairo and Giza, Egypt, and evaluated the antifungal activity, cytotoxicity, and CAP59-associated transcriptional response to zinc oxide nanoparticles (ZnO-NPs). Isolates were characterized using phenotypic methods and polymerase chain reaction (PCR) targeting the internal transcribed spacer (ITS) region. The capsule-associated gene CAP59 was assessed by PCR and transcript analysis. ZnO-NPs were synthesized and characterized using complementary physicochemical techniques. Antifungal susceptibility testing of five selected isolates revealed minimum inhibitory concentrations (MICs) of 40-60 µg/mL and minimum fungicidal concentrations (MFCs) of 60-75 µg/mL. Following exposure to ZnO-NPs at the respective MICs, reduced CAP59 transcript abundance was observed in the tested CAP59-positive isolates. Cytotoxicity assessment in PC12 cells revealed dose- and time-dependent reductions in cell viability, with IC_{50} values decreasing from 190.2 µg/mL at 24 h to 78.9 µg/mL at 72 h. These findings indicate antifungal activity of ZnO-NPs against the tested isolates, while the cytotoxicity findings highlight the need for further evaluation of their biological selectivity. The CAP59 transcriptional findings should be interpreted cautiously because measurements were performed in technical triplicates without independent biological replication and at growth-inhibitory concentrations. Further studies incorporating independent biological replicates, sub-inhibitory concentrations, and systematic selectivity assessments are needed to clarify the molecular effects and potential antifungal applications of ZnO-NPs.

Keywords: Antifungal activity; *Cryptococcus neoformans*; CAP59; Cytotoxicity; One Health; Zinc oxide nanoparticles

1. Introduction

The One Health concept emphasizes the interconnectedness of environmental, animal, and human health, particularly in the context of infectious disease transmission within agricultural and food production systems Destoumieux-Garzón, Mavingui [1]. Environmental microorganisms present in soil, water, and animal waste may act as reservoirs for opportunistic pathogens, contributing to their persistence and dissemination in urban and animal-associated environments [2, 3]. Among these microorganisms, environmental yeasts have attracted considerable attention because of their ability to survive under diverse ecological conditions [4].

Cryptococcus neoformans (*C. neoformans*) is an encapsulated environmental yeast commonly associated with soil contaminated with bird droppings, particularly those of pigeons, which provide favorable conditions for fungal survival and proliferation [5-7]. Human infection generally occurs through inhalation of airborne spores or desiccated yeast cells and may result in cryptococcosis, especially in immunocompromised individuals [8].

The pathogenicity of *C. neoformans* is strongly associated with several virulence factors, most notably the polysaccharide capsule that protects the fungus from host immune responses [9]. Capsule biosynthesis is regulated by multiple genes, including CAP59, which plays an essential role in capsule formation and fungal virulence [10]. Recently, nanomaterials have gained increasing interest as alternative antimicrobial agents. Among them, zinc oxide nanoparticles (ZnO-NPs) have demonstrated broad antifungal activity against several pathogenic fungi [11]. The antimicrobial activity of ZnO-NPs has been attributed to membrane disruption, oxidative stress induction, and interference with cellular metabolic pathways [12]. These properties highlight their potential application in controlling environmental fungal pathogens [13].

Despite the increasing interest in antifungal nanomaterials, there have been few studies that have examined the antifungal activity, cytotoxicity, and modulation of virulence-associated genes in environmental *C. neoformans* isolates following treatment with ZnO-NPs. Therefore, this study aimed to

isolate and molecularly characterize *C. neoformans* strains from pigeon droppings and assess the antifungal activity of ZnO-NPs against these isolates. Furthermore, the study explored the impact of ZnO-NPs on CAP59 gene expression to gain insight into their potential effects on fungal virulence.

2. Materials and Methods

2.1. Sample collection and fungal isolation

Bird dropping samples were collected from ten different pigeon nests located in Cairo and Giza governorates, Egypt (July, 2024). One gram of each sample was suspended in 9 mL of sterile saline solution, mixed thoroughly, and centrifuged at 3000 rpm for 5 minutes. The supernatant was discarded, and the sediment was used for fungal culture. A loopful of each processed sample was streaked onto Sabouraud dextrose agar (SDA) supplemented with chloramphenicol (5 µg/ mL) (HiMedia, India) to inhibit bacterial growth. The plates were incubated at 25°C and 37°C for 72 hours. Colonies showing a creamy, tan, or brown mucoid appearance were subcultured onto SDA slopes for further identification [14].

2.2. Phenotypic identification of yeast isolates

Phenotypic identification of suspected isolates was conducted using standard mycological techniques, which included microscopic examination with Gram staining and India ink preparation to observe capsule formation. Additional identification criteria involved assessing growth at 37°C and urease production. These procedures were carried out following the protocols outlined by Chae, Jang [15].

2.3. Molecular identification using PCR

Ten isolates suspected to be *C. neoformans* based on phenotypic characteristics were subjected to molecular identification using PCR targeting the Internal Transcribed Spacer (ITS) region.

2.3.1. DNA extraction

Genomic DNA was extracted using the QIAamp DNeasy Plant Mini Kit (Qiagen, Germany) according to the manufacturer's instructions. Briefly, 100 mg of sample was mixed with 400 µL buffer

AP1 and 4 µL RNase A solution (100 mg/mL). The mixture was disrupted using a TissueLyser system with tungsten carbide beads. After incubation at 65°C for 10 min, buffer P3 was added and the lysate was centrifuged at 14,000 rpm. The supernatant was transferred to a QIAshredder column and purified through a silica membrane column. DNA was finally eluted using 50 µL elution buffer [16].

2.3.2. PCR amplification

PCR reactions were performed in a total volume of 25 µL, containing 12.5 µL EmeraldAmp Max PCR Master Mix (Takara, Japan), 1 µL of each primer (20 pmol), 4.5 µL nuclease-free water, and 6 µL DNA template. The amplification was conducted using an Applied Biosystems 2720 thermal cycler. The primers ITS1 and CN-6 (Table 1) were used for PCR-based detection of *C. neoformans*, as previously described by [17].

Table 1. PCR-based detection of *Cryptococcus neoformans* among the tested isolates using the ITS1/CN-6 primer pair.

Target gene	Application	Primer	Sequence (5′–3′)	Amplicon size (bp)	Reference
ITS	Conventional PCR	F	TCCGTAGGTGAACCTGCGG	NR	[18]
		R	TTTAAGGCGAGCCGACGTCCTT		
CAP59	Conventional PCR	F	GAGTGTCTCCGCAACCCGCA	597	[19]
		R	CCTACTCTGCCAAATCAACTC		
CAP59	qPCR	F	AACCCGAACGAAGAAACCTC	--	[20]
		R	ACCCCAGCACCACACATACTC		
ACT1 (CNAG_00483)	qPCR/reference gene	F	CCTTGCTCCTTCTTCTAT	136	[20]
		R	CTCGTCGTATTCGCTCTT		

Internal Transcribed Spacer (ITS); NR, not reported for the ITS1/CN6 primer combination in the cited reference.

2.3.3. PCR product analysis, CAP59 detection, and gene expression analysis

PCR products obtained from conventional PCR were analyzed by electrophoresis on a 1.5% agarose gel prepared in 1× TBE buffer. A 100-bp DNA ladder (Thermo Fisher Scientific, Germany) was used as a molecular size marker. The gel was visualized and documented using a gel documentation system (Alpha Innotech, Biometra). The presence of the capsular gene *CAP59* was investigated using conventional PCR with specific primers targeting a 597-bp fragment, as described by Alarousy, Abo [19]. PCR amplification and electrophoresis were performed under the conditions described above.

Five *C. neoformans* isolates positive for the *CAP59* gene were selected for gene expression analysis. Following exposure to ZnO-NPs at the respective MIC for 24 h, total RNA was extracted using the RNeasy Mini Kit (Qiagen, Germany) according to the manufacturer's instructions and treated with DNase to remove residual genomic DNA. Complementary DNA (cDNA) was synthesized, and quantitative real-time PCR was performed using QuantiTect SYBR Green PCR Master Mix (Qiagen, Germany) on a Stratagene MX3005P real-time PCR system. *CAP59* transcript levels were normalized to the reference gene *ACT1*, and relative expression was calculated using the $^{2^{-\Delta\Delta Ct}}$ method [21], The primer sequences, expected amplicon sizes, and corresponding references are provided in Table 1. All qPCR reactions were performed in technical triplicate, and the mean Ct values of the technical replicates were used for relative-expression analysis. The results were expressed as mean ± standard error (SE) of the technical replicates.

2.4. Antifungal susceptibility testing

Antifungal susceptibility was evaluated using the disc diffusion method. The tested *C. neoformans* isolates were cultured, and standardized fungal inocula were prepared and inoculated onto the appropriate agar medium to obtain a uniform growth lawn. Antifungal discs containing the tested agents were placed on the inoculated agar surface at appropriate spacing. The plates were incubated under the conditions used for the assay, after which the diameters of the inhibition zones surrounding the discs were measured in millimeters. The inhibition-zone measurements were recorded for each isolate and antifungal agent and were interpreted descriptively. Because standardized clinical interpretive breakpoints were not applied to the inhibition-zone measurements in the present study, the results were not classified as susceptible, intermediate, or resistant.

2.5. Preparation and characterization of ZnO-NPs

2.5.1. Preparation of ZnO-NPs

ZnO-NPs were prepared using a precipitation method. Zinc acetate dihydrate (0.1 M) was dissolved in deionized water and stirred magnetically at 60 °C. Sodium hydroxide solution (0.3 M) was then added slowly under vigorous stirring, resulting in the formation of a white zinc hydroxide precipitate. The mixture was stirred for 2 h and subsequently aged for 24 h at room temperature. The precipitate was collected by centrifugation, washed with deionized water and ethanol, and dried at 80 °C for 12 h. Finally, ZnO-NPs were obtained by calcination at 400 °C for 3 h [22].

2.5.2. Characterization of ZnO-NPs

The physicochemical properties of the ZnO-NPs were evaluated using complementary analytical techniques. Scanning electron microscopy (SEM) was used to examine nanoparticle morphology and surface structure. Dynamic light scattering (DLS) was used to determine the hydrodynamic size distribution and hydrodynamic diameter of the ZnO-NPs in aqueous suspension. Fourier-transform infrared spectroscopy (FTIR) was used to characterize functional groups and surface chemical interactions. UV-visible spectroscopy (UV-Vis) was used to evaluate the optical properties, while X-ray diffraction (XRD) was used to characterize the crystalline structure and phase composition. These techniques provide complementary information for the physicochemical characterization of metal oxide nanoparticles [23, 24]

2.6. Antifungal activity of ZnO-NPs

The antifungal activity of ZnO-NPs was evaluated using the agar well diffusion method, as previously described by Kim, Sung [25], with minor modifications. Yeast suspensions were adjusted to a 0.5 McFarland standard and uniformly spread onto Sabouraud dextrose agar plates. Wells measuring 6 mm in diameter were prepared aseptically and loaded with ZnO-NPs at concentrations of 25, 50, and 100 μg per well. Ketoconazole was included as a positive antifungal control, while the corresponding nanoparticle-free treatment was used as a negative control. The plates were incubated for 48 h, after

which the diameters of the inhibition zones were measured in millimeters. The assay was performed using four replicates (n = 4), and the results were expressed as mean ± standard error (SE).

2.7. Determination of minimum inhibitory concentration (MIC) and minimum fungicidal concentration (MFC)

The antifungal susceptibility of ZnO-NPs was evaluated using the broth microdilution method in 96-well microtiter plates. Five selected *C. neoformans* isolates (isolates 1, 3, 4, 7, and 9) were tested. According to the laboratory records, ZnO-NP concentrations of 10, 20, 25, 30, 35, 40, 45, 50, 55, 60, 65, 75, 80, 85, 90, 95, and 100 µg/mL were evaluated in Mueller–Hinton broth. ZnO-NP suspensions were freshly prepared before the experiments and thoroughly vortexed to promote uniform dispersion. Following inoculation with the fungal suspension (100 µL), the plates were incubated at 27 °C for 48–72 h [26]. The MIC was defined as the lowest tested ZnO-NP concentration at which no visible fungal growth was observed. To determine the MFC, 100 µL was collected from wells showing no visible growth and subcultured onto tryptic soy agar. The plates were incubated at 27 °C for 48–72 h. The MFC was defined as the lowest concentration associated with no visible fungal growth following subculture. MIC and MFC determinations were performed in triplicate according to Espinel-Ingroff, Chaturvedi [27].

2.8.Cytotoxicity assessment of ZnO-NPs using PC12 cells

The cytotoxicity of the synthesized zinc oxide nanoparticles (ZnO-NPs) was evaluated using PC12 cells and the MTT colorimetric assay, following the principle originally described by Mosmann [28], with modifications appropriate for nanoparticle exposure. PC12 cells were cultured under standard cell-culture conditions and seeded into 96-well tissue-culture plates. After cell attachment, the cells were exposed to ZnO-NPs at concentrations ranging from 10 to 800 µg/mL for 24, 48, and 72 h. Untreated cells maintained under the same culture conditions served as the negative control. At the end of each exposure period, cell viability was determined using the MTT assay. MTT reagent was added to the wells and incubated under standard cell-culture conditions to allow viable metabolically active cells to

reduce the yellow tetrazolium salt to insoluble purple formazan crystals. The resulting formazan crystals were dissolved, and absorbance was measured using a microplate reader. Cell viability was calculated relative to the untreated control according to the following equation:

$$\textbf{\textit{Cell viability}}\ (\%) = \left[\frac{Absorbance\ of\ treated\ cells}{Absorbance\ of\ untreated\ control\ cells}\right] \times 100$$

The cytotoxicity experiment was performed in three independent replicates (n = 3), and results were expressed as mean ± standard error (SE). Concentration–response curves were generated for each exposure period, and IC_{50} values were calculated from the corresponding dose–response relationships. Because ZnO-NPs may interfere with colorimetric viability assays through light absorption, adsorption of assay components, or direct interaction with MTT, potential nanoparticle-associated interference represents an important methodological consideration when interpreting MTT-derived cytotoxicity data [29, 30].

Statistical analysis

Experiments were performed in triplicate where indicated, and results are presented as mean ± standard error (SE). Statistical analyses were performed using GraphPad Prism software version 9.0. For experiments involving independent experimental groups with appropriate biological or experimental replication, differences between groups were assessed using one-way analysis of variance (ANOVA) followed by Tukey's post hoc test, with $p < 0.05$ considered statistically significant. qPCR measurements were performed in technical triplicate, and the mean Ct values of the technical replicates were used for relative-expression analysis. Because independent biological replication was not performed for the qPCR experiment, inferential statistical testing was not applied to the CAP59 expression data; these results were interpreted descriptively.

3. Results

3.1. Isolation and phenotypic identification of yeast isolates

A total of ten pigeon dropping samples were collected from different pigeon nests located in Cairo and Giza governorates. Following culture on Sabouraud dextrose agar supplemented with

chloramphenicol, several yeast-like colonies were observed after incubation at 25 °C and 37 °C for 72 h. The colonies appeared creamy to brown with a mucoid texture. Microscopic examination using Gram staining revealed oval budding yeast cells, while India ink staining demonstrated the presence of a clear capsule surrounding the yeast cells, indicating the characteristic morphology of *C. neoformans*. The isolates also showed positive urease activity and the ability to grow at 37 °C (Figure 1).

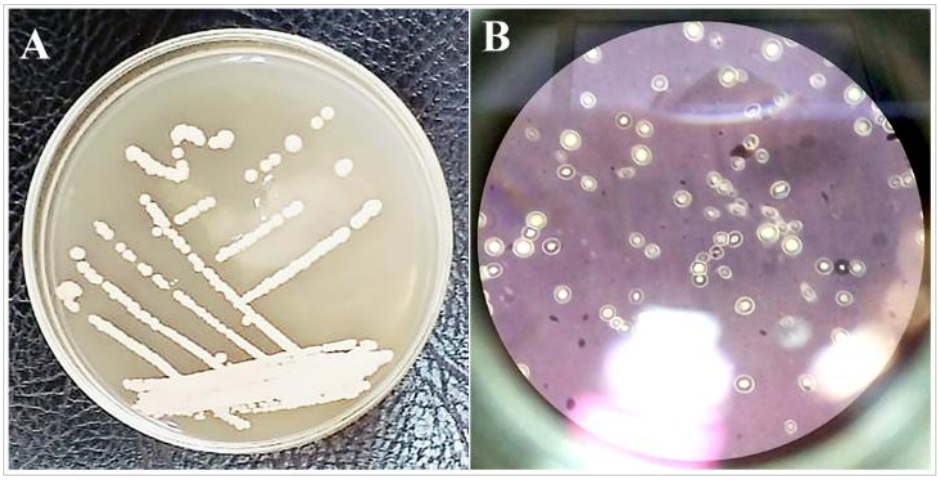

Figure 1. (**A**) *C. neoformans* on SDA after 72 h, The colonies appeared dark cream-colored, moist, shining, and mucoid. (**B**), *C. neoformans* stained with India ink stain, all isolates showed round to oval encapsulated yeast cells surrounded with clear zone.

3.2. Molecular identification of C. neoformans isolates by PCR

PCR-based detection of *C. neoformans* was performed using the ITS1/CN-6 primer pair. Seven of the ten tested isolates (1, 2, 3, 4, 6, 7, and 9) showed positive amplification, whereas isolates 5, 8, and 10 showed no amplification. Accordingly, seven isolates were classified as PCR-positive for *C. neoformans*, representing 70% of the tested samples (Table 2; Figure 2). These molecular findings were consistent with the phenotypic characteristics observed for the corresponding isolates.

Table 2. PCR amplification of the ITS region in suspected *C. neoformans* isolates using the ITS1/CN-6 primer pair.

Isolate No.	**1**	**2**	**3**	**4**	**5**	**6**	**7**	**8**	**9**	**10**
***C. neoformans* PCR detection**	+	+	+	+	-	+	+	-	+	-

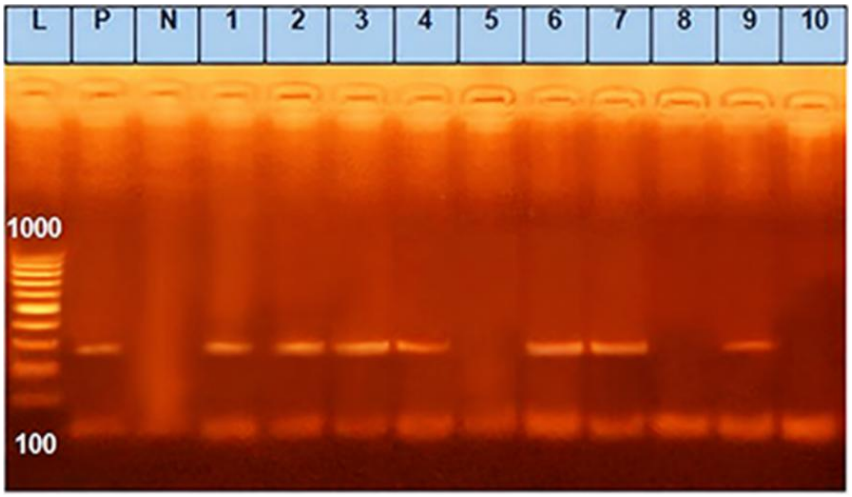

Figure 2. PCR-based detection of *Cryptococcus neoformans* among the tested isolates using the ITS1/CN-6 primer pair. Positive amplification was detected in isolates 1, 2, 3, 4, 6, 7, and 9.

3.3. Antifungal inhibition-zone profile

The antifungal susceptibility testing of *C. neoformans* isolates revealed variable inhibition-zone patterns among the tested antifungal agents (Table 3). Ketoconazole showed the largest inhibition zones, ranging from 23.3 ± 0.3 to 30.3 ± 0.3 mm, followed by clotrimazole, with inhibition zones ranging from 15.7 ± 0.3 to 23.3 ± 0.9 mm. Amphotericin B produced inhibition zones ranging from 10.7 ± 0.3 to 16.7 ± 0.3 mm, whereas itraconazole produced relatively smaller inhibition zones ranging from 10.0 ± 0.6 to 14.3 ± 0.3 mm. Voriconazole and fluconazole showed variable responses among the tested isolates, with measurable inhibition zones observed for some isolates, including isolates 3 and 7, whereas other isolates showed no detectable inhibition zones. Overall, the inhibition-zone patterns differed among the tested antifungal agents and isolates, with ketoconazole and clotrimazole producing the largest inhibition zones under the experimental conditions. Because no standardized interpretive breakpoints were applied to classify the inhibition-zone measurements, the observed absence of an inhibition zone is reported descriptively as no detectable inhibition zone rather than as clinical antifungal resistance.

Table 3. Antifungal susceptibility profile of *C. neoformans* isolates determined by the disc diffusion method.

C. neoformans isolates	Ketoconazole	Amphotericin B	Clotrimazole	Itraconazole	Voriconazole	Fluconazole
1	29.3 ± 0.3	15.0± 0.6	19.0 ± 0.6	11.0 ± 0.6	ND	ND
2	24.3 ± 0.3	14.0 ± 0.6	20.7 ± 0.3	10.7 ± 0.3	ND	ND
3	30.3 ± 0.3	14.0± 0.3	23.3 ± 0.9	14.3 ± 0.3	22.3 ± 0.9	13.3 ± 0.3
4	24.0 ± 0.6	16.7 ± 0.3	20.3 ± 0.3	10.7 ± 0.3	ND	ND
6	25.7 ± 0.3	15.7 ± 0.3	20.7 ± 0.3	10.3 ± 0.3	ND	ND

7	25.0 ± 0.6	10.7 ± 0.3	21.7 ± 0.3	11.3 ± 0.3	14.7 ± 0.3	10.7 ± 0.3
9	23.3 ± 0.3	15.3 ± 0.3	15.7 ± 0.3	10.0 ± 0.6	ND	ND

Inhibition zone diameters (mm) are presented as mean ± standard error (SE). ND = no detectable inhibition zone

3.4. Physicochemical characterization of ZnO-NPs

3.4.1. Scanning electron microscopy (SEM) Analysis

The morphology of the synthesized ZnO-NPs was examined using SEM. The SEM images revealed predominantly spherical nanoparticles with noticeable aggregation and irregular distribution, which may be attributed to their high surface energy (Figure 3). The particle size ranged from approximately 20 to 80 nm, with some larger agglomerates observed. At higher magnification, the nanoparticles appeared densely packed with clear boundaries between individual particles. These results confirm the successful synthesis of ZnO-NPs with nanoscale dimensions.

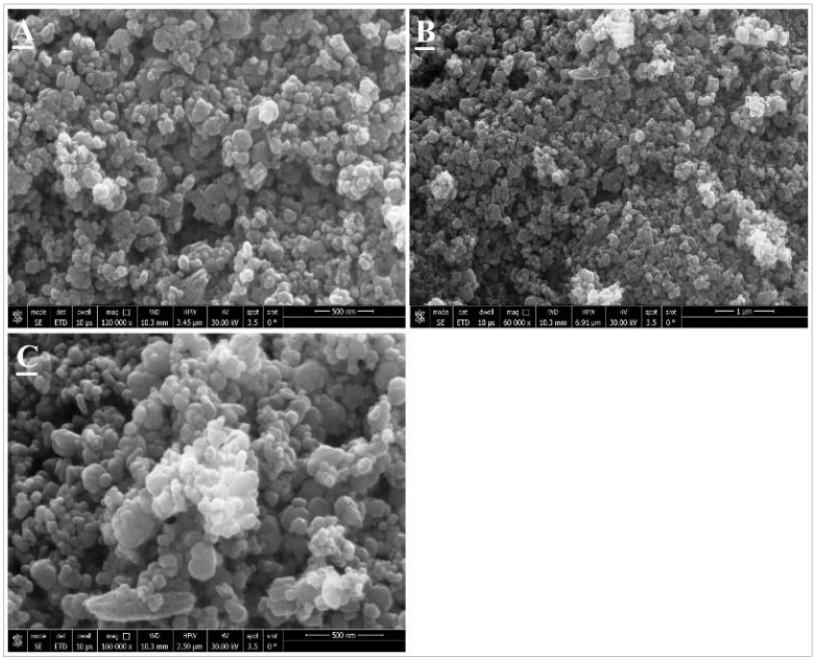

Figure 3. SEM images of synthesized ZnO-NPs at different magnifications showing the morphology and aggregation of nanoparticles. The particles appear predominantly spherical with nanoscale size distribution. (A) 60,000× magnification (scale bar = 1 μm); (B) 120,000× magnification (scale bar = 500 nm); (C) 160,000× magnification (scale bar = 500 nm).

3.4.2. Dynamic Light Scattering (DLS) Analysis

DLS analysis demonstrated that the synthesized ZnO-NPs exhibited a relatively narrow hydrodynamic size distribution in aqueous suspension. The intensity-weighted distribution displayed a dominant peak at 75.0 nm. The Z-average hydrodynamic diameter was 85.3 nm, while the polydispersity

index (PDI) was 0.218, indicating a relatively narrow size distribution. A slight tail toward larger hydrodynamic diameters indicated the presence of minor aggregation (Figure 4).

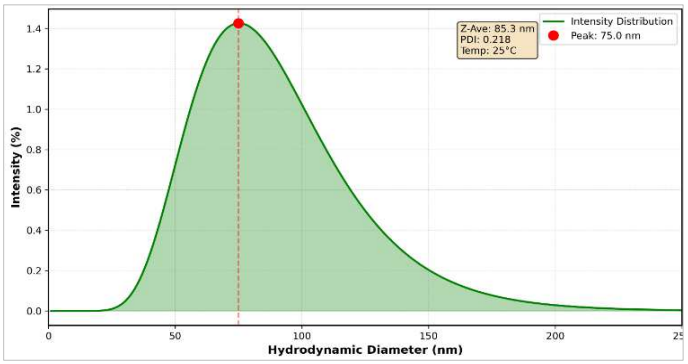

Figure 4. DLS intensity distribution of synthesized ZnO-NPs in aqueous suspension at 25 °C. The particles exhibited a dominant peak at 75.0 nm with a Z-average size of 85.3 nm and a PDI of 0.218, indicating a relatively narrow particle size distribution with minor aggregation.

3.4.3. FTIR Analysis

FTIR spectroscopy was used to identify the functional groups associated with the synthesized ZnO-NPs. A strong absorption band at ~450 cm^{-1} corresponded to Zn-O stretching vibrations, confirming the formation of ZnO-NPs. Peaks observed at ~1400 cm^{-1} and ~1600 cm^{-1} were attributed to O-H bending and C=O stretching, respectively. A band near ~2900 cm^{-1} corresponds to C-H stretching, while the broad peak at ~3400 cm^{-1} is assigned to O-H stretching, indicating the presence of hydroxyl groups or adsorbed water on the nanoparticle surface (Figure 5).

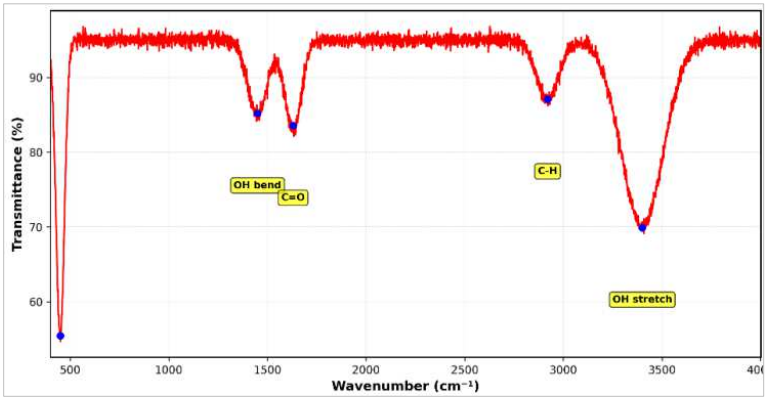

Figure 5. FTIR spectrum of ZnO-NPs showing characteristic bands corresponding to Zn-O (~450 cm^{-1}), O–H (~1400 and ~3400 cm^{-1}), C=O (~1600 cm^{-1}), and C-H (~2900 cm^{-1}) vibrations.

3.4.4. XRD Analysis

X-ray diffraction (XRD) analysis confirmed the crystalline structure of the synthesized ZnO-NPs. The diffraction pattern displayed distinct peaks at 2θ values of 31.8°, 34.5°, 36.3°, 47.5°, 56.6°,

62.8°, and 68.0°, corresponding to the crystallographic planes (100), (002), (101), (102), (110), (103), and (112), respectively. The presence of the peak at 36.3°, corresponding to the (101) plane, indicated the preferred orientation of ZnO crystals, consistent with the standard hexagonal wurtzite ZnO structure (JCPDS card No. 36-1451). The absence of impurity peaks further confirmed the high purity of the synthesized ZnO-NPs (Figure 6). Crystallite size estimation using the Scherrer equation yielded crystallite sizes ranging from approximately 25 to 31 nm, consistent with the nanoscale crystalline domains observed in the SEM analysis (Table 4).

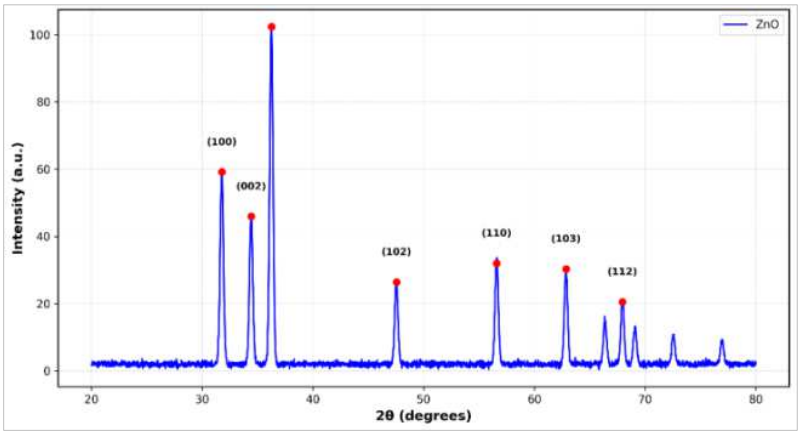

Figure 6. XRD pattern of ZnO-NPs. Diffraction peaks at 2θ values of 31.8°, 34.5°, 36.3°, 47.5°, 56.6°, 62.8°, and 68.0° correspond to the (100), (002), (101), (102), (110), (103), and (112) planes of hexagonal wurtzite ZnO (JCPDS No. 36-1451). The sharp peaks indicate high crystallinity, while the absence of additional peaks confirms phase purity.

Table 4. Crystallite size estimation of synthesized ZnO-NPs based on XRD peak analysis using the Scherrer equation.

2θ (°)	Plane	Crystallite Size (nm)
31.8	(100)	28
34.5	(002)	31
36.3	(101)	25

3.4.5. UV–Vis Spectral Analysis and Band Gap Determination

UV–Vis spectroscopy was used to evaluate the optical characteristics of the synthesized ZnO-NPs. The obtained absorption profile was consistent with the characteristic ultraviolet absorption behavior of ZnO nanoparticles (Figure 7), supporting the successful formation of ZnO-NPs. The UV–Vis spectrum, together with the FTIR, SEM, DLS, and XRD findings, confirmed the successful synthesis and physicochemical characterization of the ZnO-NPs.

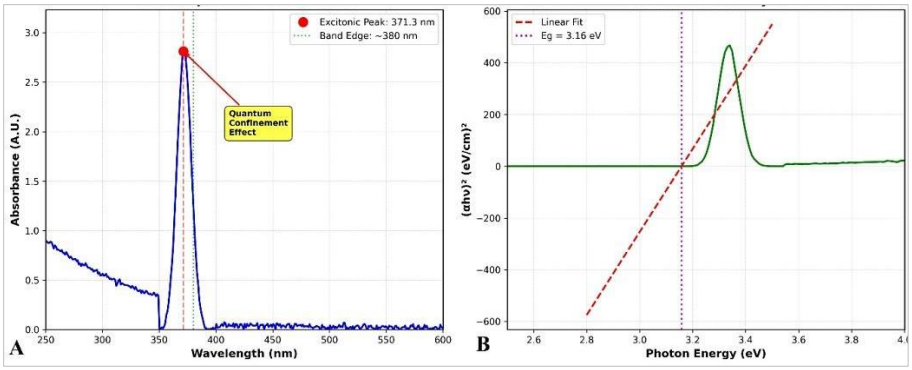

Figure 7. UV-visible absorption spectrum of ZnO-NPs. A characteristic absorption peak was observed at ~370 nm. The calculated band gap energy (~3.16 eV) confirms the typical optical properties of ZnO-NPs.

3.4.6. Zeta Potential Analysis

Zeta potential analysis was performed to characterize the surface charge and colloidal behavior of the synthesized ZnO-NPs. The nanoparticles exhibited a positive zeta potential of +28.4 ± 4.8 mV, with an average value of 27.9 mV at pH 7.0. The positive surface charge indicates the presence of a positively charged nanoparticle surface under the measurement conditions and is consistent with moderate colloidal stability. The relatively narrow distribution of zeta potential values indicates a comparatively uniform surface-charge distribution among the nanoparticles (Figure 8). The positive surface charge may facilitate electrostatic interactions with negatively charged fungal cell surfaces; however, such interactions were not directly evaluated in the present study.

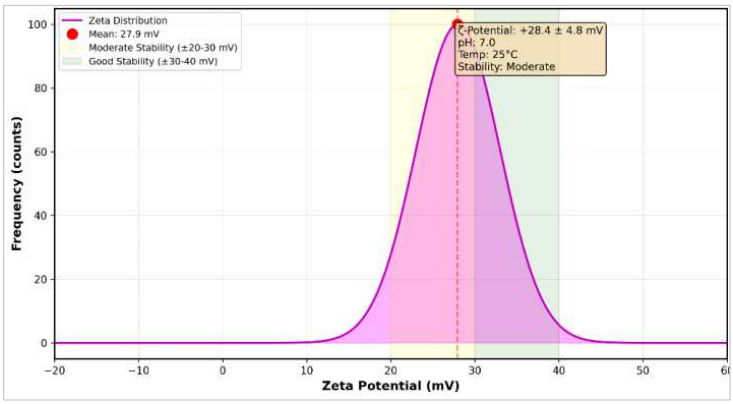

Figure 8. Zeta potential distribution of ZnO-NPs. Zeta potential analysis showed a positive surface charge of approximately +28 mV at pH 7.0, consistent with moderate colloidal stability under the measurement conditions

3.5. Cytotoxicity of ZnO-NPs in PC12 Cells

The cytotoxic effects of ZnO-NPs on PC12 cells were evaluated using the MTT assay at concentrations ranging from 10 to 800 µg/mL following exposure for 24, 48, and 72 h. Cell viability

decreased in a concentration- and exposure-time-dependent manner. At lower concentrations (10-50 µg/mL), cell viability remained above 85%, whereas exposure to higher concentrations (200–800 µg/mL) resulted in pronounced reductions in cell viability, with viability falling below 20% at the highest concentrations. The cytotoxic effect also increased with prolonged exposure. The calculated IC_{50} values decreased from 190.2 µg/mL after 24 h to 78.9 µg/mL after 72 h, indicating increased cellular sensitivity to ZnO-NPs with increasing exposure duration (Figure 9). These findings demonstrate concentration- and time-dependent cytotoxicity of ZnO-NPs in PC12 cells and emphasize the importance of dose and exposure duration when considering their potential biological applications.

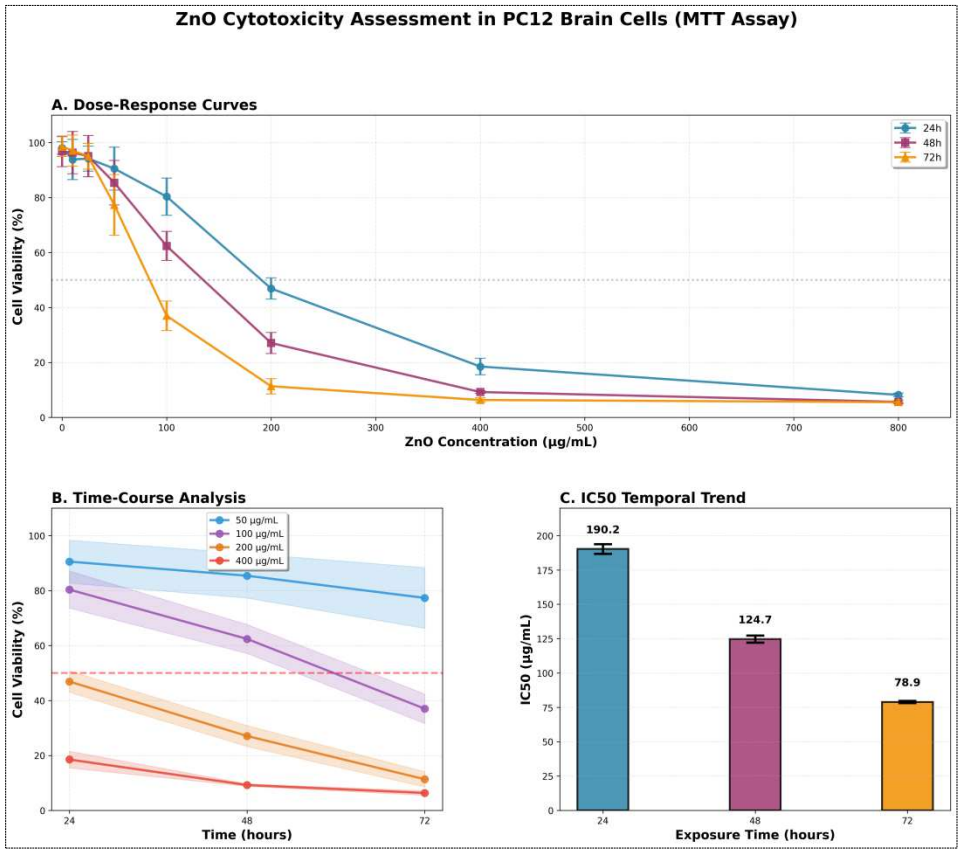

Figure 9. Cytotoxic effects of ZnO-NPs on PC12 cells. (A) Dose-dependent reduction in cell viability after 24, 48, and 72 h. (B) Time-dependent decrease in viability at selected concentrations. (C) IC_{50} values showing increased cytotoxicity with prolonged exposure. Data are presented as mean ± SE (n = 3; $p < 0.05$).

3.6. Antifungal activity of ZnO-NPs

The antifungal activity of ZnO-NPs was evaluated using the agar well diffusion method. Different concentrations of ZnO-NPs produced measurable inhibition zones against the tested *C.*

neoformans isolates. The inhibition zone diameter increased with increasing nanoparticle concentration, indicating a concentration-dependent antifungal effect (Figure 10).

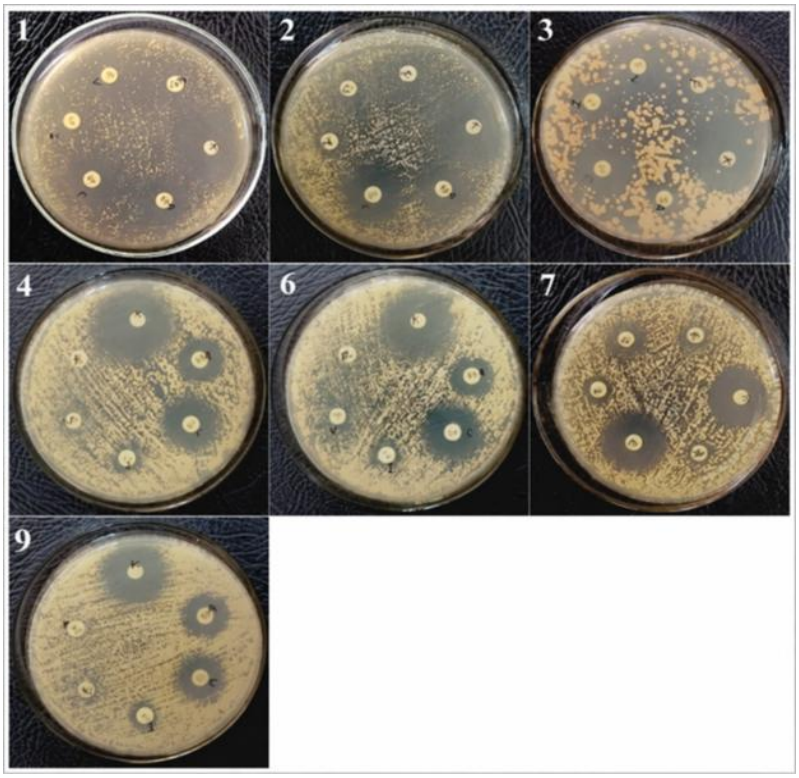

Figure 10. Agar well diffusion assay showing the antifungal activity of ZnO-NPs against *Cryptococcus neoformans* isolates 1, 2, 3, 4, 6, 7, and 9. The inhibition zones surrounding the wells indicate growth inhibition under the tested conditions.

3.7. Minimum inhibitory concentration (MIC) and minimum fungicidal concentration (MFC)

ZnO-NPs exhibited inhibitory and fungicidal activity against the five tested *C. neoformans* isolates (isolates 1, 3, 4, 7, and 9). The reported MIC values ranged from 20 to 40 µg/mL, whereas the MFC values ranged from 40 to 55 µg/mL (Table 5). Isolate 1 showed the highest MIC (40 µg/mL) and an MFC of 55 µg/mL. Isolate 9 showed the lowest MIC (20 µg/mL) and an MFC of 45 µg/mL. The differences in MIC and MFC values indicate variation in the in vitro responses of the tested isolates to ZnO-NPs.

Table 5. Minimum inhibitory concentration (MIC) and minimum fungicidal concentration (MFC) of ZnO-NPs against *C. neoformans* determined using the broth microdilution method (µg/mL).

Tested *C. neoformans* isolate	MIC (µg/ml)	MFC (µg/ml)
Isolate (1)	60	75
Isolate (3)	45	65

Isolate (4)	50	60
Isolate (7)	45	65
Isolate (9)	40	65

MIC, minimum inhibitory concentration; MFC, minimum fungicidal concentration. MIC and MFC determinations were performed for isolates 1, 3, 4, 7, and 9.

3.7. Gene expression analysis of CAP59 after ZnO treatment

Five *C. neoformans* isolates that tested positive for CAP59 were selected for real-time PCR analysis. Following exposure to ZnO-NPs at the respective MIC for 24 h, CAP59 transcript levels were lower than those observed in the corresponding untreated controls. Relative CAP59 expression after treatment ranged from 0.31 ± 0.04 to 0.58 ± 0.06. The greatest reduction was observed in isolate 3, with a 3.22-fold reduction in relative CAP59 transcript abundance. Reductions were also observed in isolates 1, 4, 7, and 9, with fold reductions of 1.72, 2.27, 2.04, and 2.70, respectively (Table 6). These findings indicate an association between ZnO-NP exposure at the MIC and reduced CAP59 transcript abundance. However, because the analysis was conducted at the MIC and was based on technical triplicate measurements, the observed differences should be interpreted descriptively rather than as evidence of statistically significant changes.

Table 6. Molecular detection and relative expression of the CAP59 gene in *C. neoformans* isolates following ZnO-NP treatment.

Sample.	*C. neoformans*	CAP59 Detection	Control Expression	Relative CAP59 Expression after ZnO-NP Treatment	Fold Reduction
1	+	+	1.00 ± 0.00	0.58 ± 0.06	1.72-fold ↓
2	+	−	ND	ND	ND
3	+	+	1.00 ± 0.00	0.31 ± 0.04	3.22-fold ↓
4	+	+	1.00 ± 0.00	0.44 ± 0.05	2.27-fold ↓
5	−	ND	ND	ND	ND
6	+	−	ND	ND	ND
7	+	+	1.00 ± 0.00	0.49 ± 0.07	2.04-fold ↓
8	−	ND	ND	ND	ND
9	+	+	1.00 ± 0.00	0.37 ± 0.05	2.70-fold ↓
10	−	ND	ND	ND	ND

+: Positive amplification
−: Negative amplification
ND: Not determined because *CAP59* was not detected.

4. Discussion

This study evaluated the environmental detection of *Cryptococcus neoformans*, its in vitro antifungal susceptibility, the antifungal activity of zinc oxide nanoparticles (ZnO-NPs), the associated changes in *CAP59* transcript abundance, and the cytotoxic effects of ZnO-NPs in PC12 cells. The findings provide preliminary evidence of the occurrence of PCR-identified *C. neoformans* in the pigeon-dropping samples examined in Cairo and Giza, together with in vitro antifungal activity of the synthesized ZnO-NPs. However, the results must be interpreted in the context of the study's limited sampling scope, the absence of sequence-based confirmation, and the experimental limitations affecting the interpretation of the gene-expression and cytotoxicity findings.

The environmental sampling was restricted to ten pigeon-dropping samples collected from pigeon nests in Cairo and Giza governorates. Phenotypic and PCR-based analyses identified seven isolates as *C. neoformans*. This finding is consistent with previous reports identifying bird-dropping-associated environments as potential ecological niches for this species [14, 31-33]. Nevertheless, the detection frequency observed in this small, geographically restricted sample cannot be considered representative of the prevalence or geographical distribution of *C. neoformans* in Cairo, Giza, or Egypt. Environmental studies have documented the occurrence and persistence of *C. neoformans* in bird-dropping-associated habitats and other environmental niches [34-36]. Such environments may provide opportunities for environmental exposure, but the present study did not investigate fungal persistence over time, aerosolization, transmission, or human exposure. Larger, systematic surveys incorporating multiple locations, seasons, and environmental sample types are therefore needed to characterize the environmental occurrence and spatial and temporal variation of this species more reliably [37-39].

Molecular identification was based on amplification of the ITS region using the ITS1/CN-6 primer pair, and the resulting findings were consistent with the phenotypic characteristics of the isolates [40]. However, sequencing confirmation was not performed. Accordingly, the isolates should be described as PCR-identified rather than sequence-confirmed *C. neoformans*. Although the observed amplification and phenotypic agreement support the identification approach used, they do not provide

the same level of confirmation as sequence-based identification or an independent validated species-specific assay [41-43]. Future studies should incorporate sequencing or an independent molecular method to strengthen species-level identification.

The antifungal susceptibility results also showed heterogeneous inhibition-zone patterns among the tested isolates, including the absence of detectable inhibition zones for some antifungal agents. Because standardized interpretive breakpoints were not applied to these measurements, the inhibition-zone results should be interpreted descriptively and should not be used to classify the isolates as clinically susceptible or resistant [44, 45]. Although antifungal resistance has been reported in environmental and clinical fungal isolates [46-48], the present findings do not establish antifungal resistance in the isolates examined. Further investigations using standardized susceptibility-testing methods and appropriate interpretive criteria, where available, would be necessary to characterize their antifungal susceptibility more rigorously.

ZnO-NPs demonstrated in vitro antifungal activity against the five selected *C. neoformans* isolates evaluated in the MIC/MFC experiments. Based on the confirmed laboratory results, the MIC values ranged from 40 to 65 µg/mL, whereas the reported MFC values ranged from 60 to 75 µg/mL. Isolate-specific differences in these values indicate variation in the responses of the tested isolates under the experimental conditions. These findings support previous reports describing the antimicrobial potential of metal oxide nanoparticles [49-52]. Nevertheless, the results are restricted to five selected isolates and should not be generalized to the broader *C. neoformans* population. In addition, the MFC value reported as 36 µg/mL requires verification against the original laboratory records because it is not included in the stated series of tested concentrations. This value should be confirmed before the manuscript is finalized.

The synthesized ZnO-NPs were characterized using complementary physicochemical techniques. FTIR analysis supported the presence of characteristic chemical bonds associated with ZnO, while UV–Vis spectroscopy showed optical absorption consistent with the synthesized material [53],SEM revealed

predominantly spherical nanoparticles with dimensions of approximately 20–80 nm, whereas DLS indicated a Z-average hydrodynamic diameter of 85.3 nm. XRD analysis supported the formation of crystalline hexagonal wurtzite ZnO, with crystallite sizes of approximately 25–31 nm estimated using the Scherrer equation [51]. These measurements are not directly interchangeable because they describe different properties: SEM provides information about particle morphology and dimensions, DLS estimates hydrodynamic size in suspension, and XRD estimates the dimensions of crystalline domains. Differences among these values are therefore not necessarily contradictory. Taken together, the results support the successful synthesis and physicochemical characterization of the ZnO-NPs, although they do not establish all properties relevant to biological performance, such as elemental composition, stability under assay conditions, or changes in particle aggregation during exposure.

The antifungal activity of ZnO-NPs may involve mechanisms previously proposed for these materials, including interactions with cellular membranes and oxidative stress [52]. However, these mechanisms were not directly investigated in the present study. Reactive oxygen species (ROS) generation was not quantified, elemental composition was not independently assessed using EDX/EDS, and ultrastructural changes were not examined by TEM. Consequently, the observed antifungal activity cannot be attributed to a specific molecular or cellular mechanism on the basis of the current data. Future investigations should combine direct ROS measurements, elemental analysis, ultrastructural imaging, and appropriate controls to distinguish among potential mechanisms and determine their relative contributions to antifungal activity.

Exposure to ZnO-NPs at the respective MICs was associated with reduced *CAP59* transcript abundance in the selected isolates. The *CAP59* gene is associated with capsule formation in *C. neoformans*, making its expression relevant to the investigation of capsule-associated biology. However, the interpretation of the present gene-expression results is limited by the experimental design. Expression was assessed following exposure at growth-inhibitory concentrations, and the measurements were based on technical triplicates without independent biological replication. Technical replicates help

assess measurement consistency but do not substitute for independent biological experiments. Therefore, the observed reduction in transcript abundance cannot be unequivocally attributed to a specific anti-virulence effect. It may also reflect growth inhibition, general cellular stress, or reduced metabolic activity associated with ZnO-NP exposure. The current results consequently indicate an association between ZnO-NP exposure and altered *CAP59* transcript abundance rather than demonstrating direct, specific modulation of capsule-associated virulence. Further studies should include independent biological replicates, exposure at sub-inhibitory concentrations, quantitative assessment of fungal growth, and direct evaluation of capsule production or phenotype. These complementary measurements would help establish whether changes in *CAP59* expression occur independently of growth inhibition and whether they correspond to measurable changes in capsule-associated characteristics.

The cytotoxicity assessment revealed a concentration- and time-dependent reduction in PC12 cell viability following ZnO-NP exposure. The IC_{50} decreased from 190.2 µg/mL at 24 h to 78.9 µg/mL at 72 h, indicating greater cytotoxicity with prolonged exposure under the experimental conditions. Similar concentration- and time-dependent effects of ZnO-NPs in PC12 cells have been reported previously [53, 54]. However, the specific cellular mechanisms responsible for the observed reduction in viability were not investigated in this study. Potential contributions from oxidative stress, mitochondrial dysfunction, and cellular uptake remain hypotheses requiring direct experimental evaluation.

The cytotoxicity results also require cautious interpretation because nanoparticle-associated optical or chemical interference may affect colorimetric MTT measurements [29, 30]. Appropriate cell-free nanoparticle controls and complementary viability assays would help determine whether the measured response reflects cellular toxicity alone or is partly influenced by assay interference. Moreover, the IC_{50} values measured in PC12 cells should not be interpreted as a direct measure of toxicity in all human cell types or as evidence of clinical safety or harm. Nevertheless, the observed cytotoxicity identifies a relevant safety concern that warrants further investigation.

Importantly, the concentrations associated with antifungal activity should be interpreted alongside the cytotoxicity findings in PC12 cells. The MIC values of ZnO-NPs ranged from 40 to 60 µg/mL, whereas the PC12-cell IC_{50} values decreased from 190.2 µg/mL after 24 h to 78.9 µg/mL after 72 h of exposure. Although the MIC values were below the measured IC_{50} values, this comparison alone does not establish a favorable therapeutic selectivity window. MIC and IC_{50} represent different biological endpoints measured in different experimental systems, and their relationship cannot establish safety or predict in-vivo efficacy. Furthermore, the time-dependent decrease in the PC12-cell IC_{50} suggests that cytotoxic effects may become more pronounced with prolonged exposure under the tested conditions. Nanoparticle properties and potential interference with in-vitro toxicity assays should also be considered when interpreting cytotoxicity data [29, 55]. Accordingly, further studies should evaluate the concentration-dependent effects of ZnO-NPs using relevant mammalian cell models, appropriate exposure conditions, and complementary cytotoxicity assays [54]. These investigations are necessary to better characterize the potential safety margins before therapeutic or other antimicrobial applications can be proposed.

Importantly, the concentrations associated with antifungal activity must be interpreted alongside the cytotoxicity findings determined by the MTT colorimetric assay in PC12 cells. While the MIC values of ZnO-NPs ranged from 40 to 60 µg/mL, the PC12 cell IC_{50} values decreased progressively over the tested exposure periods, from 190.2 µg/mL at 24 h (SI = 3.17--4.76) to 78.9 µg/mL after 72 h (SI = 1.32--1.97). Although the acute 24 h MIC values remained below the calculated IC_{50} thresholds, this comparison alone does not confirm a broad therapeutic selectivity window. Because MIC and IC_{50} represent distinct biological endpoints measured in different experimental systems (fungal cell inhibition vs. mammalian mitochondrial tetrazolium reduction), their ratio cannot conclusively prove in vivo safety or clinical efficacy. Furthermore, the time-dependent drop in PC12 cell viability highlights that cytotoxic effects become significantly more pronounced upon extended exposure (72 h). Methodological considerations, such as potential optical interference of ZnO-NPs with light absorption

at the red wavelength, adsorption of assay components, or direct chemical interaction with the MTT reagent—must also be considered when interpreting these colorimetric data [29, 30, 55]. Accordingly, further studies should evaluate the concentration- and time-dependent effects of ZnO-NPs using additional relevant mammalian cell lines, optimized exposure durations, and complementary non-colorimetric cytotoxicity assays [54] to accurately characterize safety margins prior to proposing therapeutic antimicrobial applications.

Within a broader One Health framework, the detection of PCR-identified *C. neoformans* in pigeon-dropping samples highlights the relevance of investigating environmental habitats that may contribute to fungal exposure [56]. However, this study does not establish environmental prevalence, long-term persistence, transmission, or a causal link between the sampled environments and human or animal infection. Similarly, although ZnO-NPs showed in vitro antifungal activity, their potential application for environmental fungal control cannot be inferred from laboratory efficacy alone. Any such application would require evaluation of environmental fate, dissolution and dispersion behavior, exposure, non-target effects, and ecotoxicological risks alongside antifungal effectiveness [57, 58]. Larger environmental surveys and carefully designed laboratory and environmental safety studies would be needed to assess whether nanoparticle-based approaches could have a practical role within a One Health-oriented strategy.

Several limitations should be considered when interpreting these findings. First, environmental sampling was limited to ten samples collected from selected locations in Cairo and Giza, restricting the generalizability of the findings and preventing reliable estimates of environmental prevalence. Second, molecular identification was not confirmed by sequencing. Third, antifungal susceptibility testing involved five selected isolates; therefore, the observed MIC and MFC values should be interpreted as preliminary in vitro findings rather than representative estimates for the species as a whole. Fourth, *CAP59* expression was assessed without independent biological replication, limiting the robustness of the expression analysis and preventing definitive conclusions regarding transcriptional responses or anti-

529 virulence mechanisms. Fifth, the proposed mechanisms underlying ZnO-NP antifungal activity were not
530 directly investigated through assays such as reactive oxygen species quantification or ultrastructural
531 analysis. Finally, the PC12-cell cytotoxicity assessment relied on the MTT assay, which may be subject
532 to nanoparticle-associated interference. Consequently, these results do not establish the safety,
533 therapeutic selectivity, or environmental suitability of ZnO-NPs. Further studies incorporating broader
534 environmental sampling, sequence-based identification, independently replicated gene-expression
535 experiments, mechanistic investigations, and complementary cytotoxicity and ecotoxicity assays are
536 warranted.

537 **Conclusion**

538 This study detected PCR-identified *C. neoformans* among pigeon-dropping samples collected
539 from selected locations in Cairo and Giza, highlighting the presence of this environmental yeast within
540 the sampled avian-associated habitats. Detection of the capsule-associated *CAP59* gene in five PCR-
541 positive isolates demonstrated the presence of this gene among the isolates examined. ZnO-NPs
542 exhibited in vitro antifungal activity against the five tested *C. neoformans* isolates, with reported
543 minimum inhibitory concentrations (MICs) ranging from 40 to 65 µg/mL and minimum fungicidal
544 concentrations (MFCs) ranging from 60 to 75 µg/mL. Exposure to ZnO-NPs at the respective MICs was
545 associated with reduced *CAP59* transcript abundance. Because *CAP59* expression was assessed under
546 growth-inhibitory conditions, the observed reduction may reflect both effects associated with ZnO-NP
547 exposure and general cellular stress or reduced metabolic activity. Therefore, these findings provide
548 preliminary evidence of an association between ZnO-NP exposure and altered *CAP59* expression rather
549 than definitive evidence of a specific anti-virulence effect. In addition, the cytotoxicity observed in
550 PC12 cells, including a decrease in the IC_{50} from 190.2 µg/mL at 24 h to 78.9 µg/mL at 72 h, highlights
551 the importance of evaluating nanoparticle concentration, exposure duration, and biological selectivity.
552 Further studies using sub-inhibitory ZnO-NP concentrations, independent biological replicates,
553 quantitative assessment of fungal growth and capsule phenotype, complementary molecular analyses,

and comprehensive safety evaluation are required to clarify the mechanisms underlying the antifungal activity and *CAP59*-associated response of ZnO-NPs.

Declaration

Funding

This research received no external funding.

Authors Contributions

Mona M. H. Soliman: Conceptualized the study, performed the experiments, analyzed the data, and drafted the manuscript**. Mai M. Kandil**: Contributed to sample collection, microbiological and molecular analyses, and assisted in data interpretation**. Mohamed Seif:** Conceptualized the study, Contributed to nanoparticle synthesis and characterization, and writing– review & editing. All authors read and approved the final version of the manuscript.

Conflict of interest

The authors declare no conflicts of interest.

Acknowledgements

The authors gratefully acknowledge the Departments of Microbiology and Immunology and Food Toxicology and Contaminants at the National Research Centre, Egypt, for their support and for providing access to laboratory facilities. This research did not receive any specific funding.

Data availability

Data will be made available on request.

Ethical Statement

This study did not involve the use of animals or human subjects; therefore, ethical approval was not required.

Copyright and Permissions

All figures and tables presented in this manuscript are original and created by the authors. No previously published or copyrighted material has been used, and therefore no permissions were required

References

1. Destoumieux-Garzón, D., et al., *The one health concept: 10 years old and a long road ahead.* 2018. **5**: p. 14.
2. Banerjee, S. and M.G.J.N.R.M. Van Der Heijden, *Soil microbiomes and one health.* 2023. **21**(1): p. 6-20.
3. Mahunu, G., et al., *Safe food handling techniques to prevent microbial contamination*, in *Food safety and quality in the global south*. 2024, Springer. p. 427-461.
4. Botha, A.J.S.B. and Biochemistry, *The importance and ecology of yeasts in soil.* 2011. **43**(1): p. 1-8.
5. THOMES, L., *PREVALENCE OF CRYPTOCOCCUS NEOFORMANS IN MAN, ANIMAL AND ENVIRONMENT*. 2004, ANAND AGRICULTURAL UNIVERSITY.
6. Samarasinghe, H., *Global Distribution, Epidemiology and Genetics of Infectious Yeast Cryptococcus deneoformans and Other Soil Yeasts*. 2021.
7. Mia, M.M., M. Hasan, and M.R.J.H. Hasnath, *Global prevalence of zoonotic pathogens from pigeon birds: A systematic review and meta-analysis.* 2022. **8**(6).
8. Zhao, Y., et al., *Cryptococcus neoformans, a global threat to human health.* 2023. **12**(02): p. 1-18.
9. Araújo, G.R.d.S., et al., *The environmental yeast Cryptococcus liquefaciens produces capsular and secreted polysaccharides with similar pathogenic properties to those of C. neoformans.* 2017. **7**(1): p. 46768.
10. Al-Huthaifi, A.M., et al., *Mechanisms and virulence factors of Cryptococcus neoformans dissemination to the central nervous system.* 2024. **10**(8): p. 586.
11. Emam, M., et al., *Green Synthesis of Curcuminoids-Enriched Trimetallic Nanoparticles Stabilised by Chitosan/Collagen Nanocomposites against Foodborne Pathogens.* 2026: p. 1-22.
12. Yang, J., D. Xiong, and M.J.N. Long, *Zinc oxide nanoparticles as next-generation feed additives: Bridging antimicrobial efficacy, growth promotion, and sustainable strategies in animal nutrition.* 2025. **15**(13): p. 1030.
13. Mahamuni-Badiger, P., et al., *The fungal infections and their inhibition by Zinc oxide nanoparticles: an alternative approach to encounter drug resistance.* 2024. **67**(2): p. 291-309.
14. Sirag, B., et al., *Cryptococcus neoformans and other opportunistic Cryptococcus species in pigeon dropping in Saudi Arabia: identification and characterization by DNA sequencing.* 2021. **12**: p. 726203.
15. Chae, H., et al., *Classification of Cryptococcus neoformans and yeast-like fungus isolates from pigeon droppings by colony phenotyping and ITS genotyping and their seasonal variations in Korea.* 2012. **56**(1): p. 58-64.
16. Abdel-Latif, A. and G.J.P.m. Osman, *Comparison of three genomic DNA extraction methods to obtain high DNA quality from maize.* 2017. **13**(1): p. 1.
17. Mitchell, T.G., et al., *Unique oligonucleotide primers in PCR for identification of Cryptococcus neoformans.* 1994. **32**(1): p. 253-255.
18. Hamzehee, S., et al., *Geographical distribution of Cryptococcus neoformans in Iran, pathogenic factors, and antifungal susceptibility profile.* 2025. **25**(1): p. 522.
19. Alarousy, R., et al., *Amplification of capsule-associated genes from Cryptococcus neoformans.* 2011. **4**: p. 1-5.
20. Fonseca, F.L., et al., *Binding of the wheat germ lectin to Cryptococcus neoformans chitooligomers affects multiple mechanisms required for fungal pathogenesis.* 2013. **60**: p. 64-73.
21. Livak, K.J. and T.D.J.m. Schmittgen, *Analysis of relative gene expression data using real-time quantitative PCR and the 2− ΔΔCT method.* 2001. **25**(4): p. 402-408.
22. Osman, D.A.M. and M.A.J.J.N.N. Mustafa, *Synthesis and characterization of zinc oxide nanoparticles using zinc acetate dihydrate and sodium hydroxide.* 2015. **1**(4): p. 248-251.
23. Sirelkhatim, A., et al., *Review on zinc oxide nanoparticles: antibacterial activity and toxicity mechanism.* 2015. **7**(3): p. 219-242.
24. Kumar, A., et al., *Engineered ZnO and TiO2 nanoparticles induce oxidative stress and DNA damage leading to reduced viability of Escherichia coli.* 2011. **51**(10): p. 1872-1881.

25. Kim, K.-J., et al., *Antifungal activity and mode of action of silver nano-particles on Candida albicans.* 2009. **22**(2): p. 235-242.
26. Barchiesi, F., et al., *Turbidimetric and visual criteria for determining the in vitro activity of six antifungal agents against Candida spp. and Cryptococcus neoformans.* 1993. **124**(1): p. 19-25.
27. Espinel-Ingroff, A., et al., *Optimal testing conditions for determining MICs and minimum fungicidal concentrations of new and established antifungal agents for uncommon molds: NCCLS collaborative study.* 2002. **40**(10): p. 3776-3781.
28. Mosmann, T.J.J.o.i.m., *Rapid colorimetric assay for cellular growth and survival: application to proliferation and cytotoxicity assays.* 1983. **65**(1-2): p. 55-63.
29. Kroll, A., et al., *Interference of engineered nanoparticles with in vitro toxicity assays.* 2012. **86**(7): p. 1123-1136.
30. Doak, S., et al., *Confounding experimental considerations in nanogenotoxicology.* 2009. **24**(4): p. 285-293.
31. Taha, M., et al., *Genetic diversity and antifungal susceptibilities of environmental Cryptococcus neoformans and Cryptococcus gattii species complexes.* 2024. **15**(1): p. 21.
32. Oghomwenakhin, E., L.J.N.J.o.B. Eboigbe, and A. Sciences, *Screening and selection of Cryptococcus neoformans using urease activity and temperature range.* 2019. **27**(2): p. 57-61.
33. Velagapudi, R., et al., *Spores as infectious propagules of Cryptococcus neoformans.* 2009. **77**(10): p. 4345-4355.
34. Hagen, F., et al., *Importance of resolving fungal nomenclature: the case of multiple pathogenic species in the Cryptococcus genus.* 2017. **2**(4): p. 10.1128/msphere. 00238-17.
35. May, R.C., et al., *Cryptococcus: from environmental saprophyte to global pathogen.* 2016. **14**(2): p. 106-117.
36. Rajasingham, R., et al., *Global burden of disease of HIV-associated cryptococcal meningitis: an updated analysis.* 2017. **17**(8): p. 873-881.
37. Pouris, J., et al., *The role of fungi in food production and processing.* 2024. **14**(12): p. 5046.
38. Bintsis, T.J.A.m., *Microbial pollution and food safety.* 2018. **4**(3): p. 377.
39. Alegbeleye, O.O., I. Singleton, and A.S.J.F.m. Sant'Ana, *Sources and contamination routes of microbial pathogens to fresh produce during field cultivation: A review.* 2018. **73**: p. 177-208.
40. Kidd, S.E., et al., *A new age in molecular diagnostics for invasive fungal disease: are we ready?* 2020. **10**: p. 2903.
41. Rodrigues, M.L., et al., *Pathogenicity of Cryptococcus neoformans: virulence factors and immunological mechanisms.* 1999. **1**(4): p. 293-301.
42. Casadevall, A.J.V., *Pathogenicity and virulence of Cryptococcus neoformans from an environmental perspective.* 2025. **16**(1): p. 2547090.
43. Kronstad, J., et al., *Adaptation of Cryptococcus neoformans to mammalian hosts: integrated regulation of metabolism and virulence.* 2012. **11**(2): p. 109-118.
44. Akinosoglou, K., et al., *Amphotericin B in the era of new antifungals: where will it stand?* 2024. **10**(4): p. 278.
45. Bratton, E.W., et al., *Approaches to antifungal therapies and their effectiveness among patients with cryptococcosis.* 2013. **57**(6): p. 2485-2495.
46. Jadhav, J.J., et al., *Ultrasound-assisted hydrodistillation for extraction of essential oil from clove buds–a step towards process improvement and sustainable outcome.* 2023. **189**: p. 109404.
47. Slavin, Y.N., et al., *Metal nanoparticles: understanding the mechanisms behind antibacterial activity.* 2017. **15**(1): p. 65.
48. Beyth, N., et al., *Alternative antimicrobial approach: nano-antimicrobial materials.* 2015. **2015**(1): p. 246012.
49. Dizaj, S.M., et al., *Antimicrobial activity of the metals and metal oxide nanoparticles.* 2014. **44**: p. 278-284.
50. Djearamane, S., et al., *Antifungal properties of zinc oxide nanoparticles on Candida albicans.* 2022. **12**(12): p. 1864.

51. Ismail, M., et al., *ZnO nanoparticles: Surface and X-ray profile analysis.* 2018. **14**(5): p. 381-393.
52. Westman, J., B. Hube, and G.D.J.C.m. Fairn, *Integrity under stress: Host membrane remodelling and damage by fungal pathogens.* 2019. **21**(4): p. e13016.
53. Liang, H., et al., *Neuroinflammation is induced by tongue-instilled ZnO nanoparticles via the Ca2+-dependent NF-κB and MAPK pathways.* 2018. **15**(1): p. 39.
54. Suthar, J.K., A. Vaidya, and S.J.B.T.E.R. Ravindran, *Size, Surface Properties, and Ion Release of Zinc Oxide Nanoparticles: Effects on Cytotoxicity, Dopaminergic Gene Expression, and Acetylcholinesterase Inhibition in Neuronal PC-12 Cells: JK Suthar et al.* 2024. **202**(5): p. 2254-2271.
55. Love, S.A., et al., *Assessing nanoparticle toxicity.* 2012. **5**(1): p. 181-205.
56. Abulreesh, H.H., et al., *First report of environmental isolation of Cryptococcus neoformans and other fungi from pigeon droppings in Makkah, Saudi Arabia and in vitro susceptibility testing.* 2015. **5**(8): p. 622-626.
57. Ellis, D. and T.J.T.L. Pfeiffer, *Ecology, life cycle, and infectious propagule of Cryptococcus neoformans.* 1990. **336**(8720): p. 923-925.
58. OECD, *Guidance document for the testing of dissolution and dispersion stability of nanomaterials and the use of the data for further environmental testing and assessment strategies. Series on Testing and Assessment, No. 318.* 2020.

Supplementary Files

This is a list of supplementary files associated with this preprint. Click to download.

- Samplementryfile.docx